frontiers | Frontiers in Mechanical Engineering

TYPE Original Research
PUBLISHED 06 January 2026
DOI 10.3389/fmech.2025.1729043

OPEN ACCESS

EDITED BY
Vijay Raghunathan,
King Mongkut's University of Technology North Bangkok, Thailand

REVIEWED BY
Chitaranjan Pany,
Vikram Sarabhai Space Centre, India
Jafrey Daniel James D.,
K. Ramakrishnan College of Engineering (KRCE), India

*CORRESPONDENCE
Amjed H. Albayati,
a.khalil@uobaghdad.edu.iq

RECEIVED 20 October 2025
REVISED 27 November 2025
ACCEPTED 28 November 2025
PUBLISHED 06 January 2026

CITATION
Hmoad NR, Ali AH, Saadoon AM, Abdulkareem AA and Albayati AH (2026) Effect of different wing geometries on their vibration characteristics.
Front. Mech. Eng. 11:1729043.
doi: 10.3389/fmech.2025.1729043

Effect of different wing geometries on their vibration characteristics

Nassear R. Hmoad[1], Anmar H. Ali[1], Ali Malik Saadoon[1], Aveen A. Abdulkareem[2] and Amjed H. Albayati[3]*

[1]Department of Aeronautical Engineering, University of Baghdad, Baghdad, Iraq, [2]Department of Mechanical Engineering, University of Baghdad, Baghdad, Iraq, [3]Department of Civil Engineering, University of Baghdad, Baghdad, Iraq

Understanding how wing geometry and internal structural configuration influence vibration behavior is essential for ensuring the aeroelastic stability and structural integrity of modern aircraft. This study presents a comprehensive numerical investigation of the modal and deflection characteristics of aircraft wings with different geometries (symmetric tapered planform and swept-back) and spar configurations (box and I-section) using the finite element method (FEM) in ANSYS Mechanical APDL R.15. Six NACA airfoil profiles (0024, 2411, 2416, 2424, 4412, and 4421) with angle of attack 9° under 50 m/s speed and 1,100 kg pay load were analyzed under identical aerodynamic and material conditions using linear elastic and small-deformation theory. Aerodynamic coefficients were determined using thin airfoil and Prandtl's lifting-line theories, while modal parameters were extracted through high-order 20-node solid brick elements and verified through mesh convergence analysis. Based on the results obtained, the tapered wings show a natural frequency nearly 22% higher than swept-back wings. The matter that confirms the dominant influence on geometric stiffness. On the other hand box spar wings reveal 9.5%–22% higher frequencies but showed 20%–30% higher deflection than I-section spars, demonstrating their superior torsional compliance and enhanced energy absorption under the dynamic effect. On the contrary, I-section spar resulted in higher bending stiffness and lower deformation, especially in higher-order modes. Based on airfoil series, the more the thick NACA 0024 as well as 2424 profiles revealed the highest levels of stiffness, based on 6th mode frequency that exceeded 250 Hz, but the thinner cambered sections like NACA 4412 and 4421 exhibited compliance and limited rigidity against torsion. Based on the findings, the obtained increase in the natural frequency and the reduced deflection with stiffer geometries reflect improved resistance to aeroelastic instability like flutter onset. A statistical analysis using ANOVA verified that the geometry of the wing has a statistically more significant effect on modal response than the spar type although both have a significant influence on vibration behavior. Furthermore, the result of analysis concludes that the taper wings reinforced with spars type I-section give the most balanced combination of weight efficiency, stiffness and stability against vibration for the aircraft type medium payload.

KEYWORDS

aerodynamic, box spar, I-spar, mode shape, wing vibration

1 Introduction

In aerospace structural design, the vibration properties of aircraft wings are still a major concern due to their direct effect on aeroelastic stability, fatigue life, and hence the safety of flight. Interference among the structural stiffness, aerodynamic forces as well as inertial effects yields a complex bending and torsion coupling behavior which could result in resonance and flutter if not properly eliminated (Patil and Patil, 1997). The precise estimation of modal parameters, which includes natural frequency, mode coupling and deflection shapes, is therefore central for ensuring structural reliance based on variable condition of flight. In the last three decades, an understanding of the dynamic response of wings with varying platform geometry, martial composition and internal structures has significantly progressed. The analysis conducted earlier by (Patil and Patil, 1997; Jha et al., 1997) established the basics of aeroelastic coupling in composite wings, the matter which reveals how the angle of sweep influences the critical flutter speed. A continuous development, specifically the introduction of the FEM and the dynamic stiffness method (Pagani et al., 2014; Banerjee, 2016; Viglietti et al., 2017), enable the highly precise prediction of modal behavior in slender and multi-cell wing structures.

The spar element plays the key role in reducing wing vibration. Previous studies (Sedaghati et al., 2006; Miskin and Takahashi, 2019; Pany et al., 2001) revealed that box spars provide superior torsional stiffness and higher natural frequencies than their counterparts I-shaped spars, which have in turn lower deflection values. The analytical and experimental studies validate such behavior (Demirtaş and Bayraktar, 2019; Hoy et al., 2023; Pany, 2023). The effect of material anisotropy and structural arrangements on the fluttering margin was documented to reduce it by about 20% (Guo et al., 2006; Jonsson et al., 2023; He et al., 2023).

Nonlinear behavior of tapered swept wings was investigated by (Patuelli et al., 2024; Elshazly et al., 2025) using computational fluid dynamics- coupled aeroelasticity. Studies on biomimetic configurations (Basak and Akdemir, 2024) and optimizing composite wings (Rajamurugu et al., 2024) showed that innovative selection of geometric characters leads to simultaneous improvement in aerodynamic performance and dissipating vibration energy. Despite this progress, a comprehensive comparison addressing the combined influence of wing geometry (tapered vs. swept) and spar configuration (box vs. I-section) under uniform boundary and material conditions remains limited.

To fulfill the gap in the existing literature, the current work investigates the influence of different geometries of wings on vibration behavior using FEM. Two types of symmetric wings (taper and swept) supported with box and I-section spars using 6 NACA (The National Advisory Committee for Aeronautics) wing types (0024, 2411, 2416, 2424, 4412, 4421) were implemented. Furthermore, natural frequencies, mode shapes and deflection behavior under a certain structure and aerodynamic parameters were evaluated. The main objective was to quantify how the geometric and internal design parameters synergistically shape the model behavior of aircraft wings, providing a clear understanding of their potential for aeroelastic optimization. The models studied were carefully selected to highlight the two main parameters: wing thickness and curvature in terms of camber values. The addressed cases had a variable thickness-to-cord ratio that ranged from 11% to 24% while the deviation in camber was 4%. A concise summary of key contributions from previous studies is presented in Table 1, highlighting methodological evolution, comparative findings, and persistent research gaps that underpin the motivation for the present analysis.

2 Methodology

This section outlines the numerical methodology employed to investigate the influence of wing geometry on vibration characteristics through a comprehensive FEM analysis. The simulations were performed using ANSYS Parametric Design Language (APDL R15), which provides a reliable platform for extracting natural frequencies and mode shapes in complex three-dimensional aerospace structures. This approach allows accurate assessment of the structural stiffness and modal coupling effects associated with different wing configurations. The aerodynamic behavior of each wing was analyzed using the thin airfoil theory and Prandtl's lifting-line theory, which relate the aerodynamic circulation to the angle of attack and spanwise lift distribution for finite wings.

The input data are aircraft weight, air density, speed and NACA wing models, their planform, cord length and angle of attack to evaluate the aerodynamic coefficients for each configuration based on these theories to characterize the adequate wing length. These values are considered the light weight - general aviation and training airplanes, where their working characteristics are: taper ratio (0.35–0.6), speed (40–75 m/s) in addition to the weight range (600–1,200 kg) and cord length (0.9–1.2 m).

The aerodynamic coefficients were determined for each configuration based on these theories to characterize the aerodynamic loading conditions applied within the FEM environment. The structural and aerodynamic analyses were integrated within a unified computational framework to find the combined influence of geometry, material properties, and boundary conditions on the modal response. Two primary wing planform configurations, tapered and swept-back, were modeled under identical mechanical and aerodynamic parameters to isolate geometric effects. Modal parameters, including natural frequencies, mode shapes, and deflection patterns, were extracted for each configuration. All numerical results were validated against established analytical data, confirming the accuracy, convergence, and physical reliability of the developed model.

3 Fluid–structure interaction governing equations

The governing equations the motion of the fluid domain are the incompressible Navier-Stokes equations, and the equations that govern the structural response are the dynamic equilibrium equation of elasticity. The fluid equations (Equations 1, 2) can be formulated as:

$$\nabla \cdot u = 0 \tag{1}$$

$$\rho_{ff}\left(\partial u/\partial t + u\left(\left(u - u_m\right)\cdot\nabla\right)\right) = -\nabla p + \mu_f \nabla^2 u \tag{2}$$

Where u is the fluid velocity, um is the mesh velocity (from structural deformation), p is pressure, and ρ_f, μ_f are the fluid density and viscosity.

TABLE 1 Chronological summary of key studies on wing geometry, spar configuration, and modal performance.

References	Wing/model type	Method/tool	Key findings	Relevance
Jha et al. (1997)	Composite box beam, taper and sweep	FEM	Ply orientation + sweep alter flutter/ divergence speeds	Early geometry–material coupling
Patil and Patil (1997)	Swept composite beam	Analytical	Ply layup changes critical flutter speeds	Fundamental aeroelastic coupling
Klimmek and Schwochow (2001)	High-aspect-ratio composite wing	Aeroelastic code (LS-DYNA)	Aspect ratio ↑ → flutter margin ↑	Geometric influence baseline
Guo et al. (2006)	Swept–tapered composite wing box	Tailoring study	Layup optimization ↑ flutter speed >20%	Material–geometry synergy
Hongwei and Mao (2008)	Composite box beam	Analytical + FEM	Bending–torsion coupling via anisotropy	Mechanistic validation
Choi et al. (2013)	Swept tapered composite wing	FEM + CFD	Sweep shifts coupling → flutter delay	Sweep influence
Campos and Marta (2013)	Metallic & composite wings	Modal testing + FEM	Experimental mode-shape validation	Empirical benchmark
Ahmed and Ahmed (2014)	Tapered wing beam	FEM	Mode-shape comparison for AR variations	Structural tuning
Pagani et al. (2014)	Multi-cell composite wing	1-D refined beam FEM	Accurate modal shapes vs. 3-D shell	High-order FEM validation
Banerjee (2016)	Composite aeroelastic beam	Dynamic-stiffness method	Efficient coupled-mode prediction	Computational efficiency
Viglietti et al. (2017)	Multi-cell tapered composite wing	Higher-order FEM	Accurate frequency prediction	Benchmark FEM study
Chan et al. (2018)	Composite box beam	Aeroelastic tailoring	Fiber orientation tunes modal coupling	Structural tailoring
Su and Banerjee (2018)	High-aspect-ratio wing	Refined dynamic-stiffness	Improved modal accuracy for slender wings	Extended slender-wing modeling
Bennamia et al. (2018)	Composite swept wing	3-D FEM	Nonlinear modal interaction quantified	Nonlinear mode study
Miskin and Takahashi (2019)	Torque-box wing	FEM	Box spars ↑ stiffness & flutter speed	Spar-stiffness comparison
Farsadi and Hasbestan (2019)	Swept composite tapered wing	Thin-walled FEM	Ply angle ↑ flutter/divergence limits	Confirms anisotropic effect
Demirtaş and Bayraktar (2019)	NACA 4415 cantilever wing	Analytical + FEM	Beam results ≈ FEM; validates models	Validation reference
Srividhya et al. (2020)	Swept wing	FEM + flutter analysis	Sweep ↔ bending–torsion coupling	Confirms sweep effect
Jonsson et al. (2023)	Tailored composite layups	FEM + optimization	Curvilinear laminates ↑ flutter >20%	Advanced composite tailoring
Patuelli et al. (2023)	Multi-cell composite wing	Unified FEM	Accurate nonlinear modal behavior	Modern nonlinear FEM
Krishna et al. (2023)	Eppler 171 & Selig S6062 wings	ANSYS 2022 R2	10 modes analyzed; Al stable modal behavior	Profile-comparison dataset
He et al. (2023)	Swept tapered composite	CFD–FEM coupling	Taper ↑ freq. 12%; validated aeroelastic model	Taper effect quantification
BASAK and Akdemir (2024)	Biomimetic Cessna 172	CFD + FEM	15% glide ratio ↑; deformation ↓	Bio-inspired optimization
Rajamurugu et al. (2024)	Composite morphing wing	Nonlinear FEM	Ignoring coupling → instability underestimation	Motivation for unified models
Patuelli et al. (2024)	Multi-tapered composite wing	Unified FEM + optimization	Integrated aeroelastic tailoring	Latest unified modeling
Elshazly et al. (2025)	Composite swept wing	CFD–FEM coupling	Nonlinear coupling ↑ flutter accuracy; taper ↑ freq 12%	Modern high-fidelity benchmark

The structural dynamics of the deformable airfoil surface are governed by the equation of motion (Equation 3) for elastic solids:

$$f_{ext} = C\partial d/\partial t + \rho_s \partial^2 d/\partial t^2 + Kd \quad (3)$$

Where d is the displacement vector, ρ_s is the structural density, C is the damping matrix, K is the stiffness matrix and f_{ext} represents the external aerodynamic loads transferred from the fluid.

4 Coefficients of aerodynamic wing forces

As air passes around the wing, and due to its angle of attack and camber, with the presence of dynamic pressure from speed and density, a pressure difference occurs between the upper and lower wing surfaces. The resultant force directed between the wind

TABLE 2 Aerodynamic and geometric date for tapered wings at 9° angle of attack.

NACA wing model	0024	2411	2416	2424	4412	4421
Coefficient of lift, C_L	0.9001	1.1875	1.2150	1.2747	1.5912	1.6671
Surface area, S (m^2)	7.8291	5.9344	5.8000	5.5287	4.4288	4.2271
Wing length (m)	9.2107	6.9816	6.8235	6.5043	5.2104	4.9731

TABLE 3 Aerodynamic and geometric date for swept wings at 9° angle of attack.

NACA wing model	0024	2411	2416	2424	4412	4421
Coefficient of lift C_L	0.7829	1.0303	1.0531	1.1023	1.3721	1.4331
Surface area S (m^2)	9.0019	6.8402	6.6917	6.3933	5.1362	4.9175
Wing length (m)	9.0019	6.8402	6.6917	6.3933	5.1362	4.9175

direction and the vertical, acting as lift, is translated by the wing area into a two-component force: lift and drag. This is the fundamental principle of flight. Swept-back wings are better in comparison to other wings, especially to swept-forward wings in their drag force. Laboratory and on-site tests used to compare wing performance face the problem of the variations in size and shape between different wing types. Therefore, it was necessary to find a standard that reduces differences and unifies the method of evaluating wings in terms of lift, drag, and torque. This is why the lift and drag performance of wings is evaluated using dimensionless numbers that minimize the effects of shape differences (Ahmed et al., 2025). Wing coefficients are dimensionless dynamic coefficients derived using the Fast Fourier Transform (FFT) to relate the angle of attack to the rotation around the wing, based on the ideal potential flow state of constant density, with no internal friction and no rotation (Liu, 2021). The general form of the lift coefficients is presented in Equations 4–7 as below.

$$C_L = a(\alpha - \alpha_0) \tag{4}$$

$$a = \frac{a_0}{1 + \frac{a_0}{\pi AR e}} \tag{5}$$

$$C_D = C_{D0} + k C_L^2 \tag{6}$$

$$k = \frac{1}{\pi e AR} \tag{7}$$

Where C_L is the coefficient of lift, C_D is the coefficient of drag and α is the angle of attack, C_{D0} is the coefficient of drag at (α_0) zero lift angle of attack, while the slop of the curve of coefficient C_L versus angle of attack, AR is the aspect ratio and **e** is Oswald constant, a_0 Two-Dimensional Airfoil Lift Slope

5 Wing geometries and classifications

The three main structural components of the wing, spar, ribs, and skin, provide an ideal balance between strength, flexibility, and load distribution. Spar, with its high resistance to bending and torsion, is the reason for the wing's stability and resistance to dynamic forces. Ribs transfer forces from the wing surface to the spar and support the skin surface shape, providing high flexibility and wing surface dent resistance. Skin distributes aerodynamic forces smoothly and contributes to enhanced torsional rigidity. The synergy of these three parts gives the structure high flexibility, uniform force distribution, and reinforcement, while also achieving efficient mass distribution.

In general, aircraft are designed to meet specific requirements and need efficient aerodynamic conditions to achieve them, along with exceptional structural resilience to survive and withstand these conditions. Accordingly, the design process determines the wing surface shape, cross-section, position on the fuselage, length, root width, and taper. The aircraft's maneuverability, speed limits, stability, payload, runway length, takeoff and landing performance, are additional constraints that place strict limitations on the internal structure and external shape of the wings (Jaafar and Hmoad, 2024).

Wings are classified depending on wing surface shape or what so called the planform front view, position on the fuselage, and their cross sections. The main types of wings are rectangle, taper, swept back, swept forward, dihedral, anhedral, and they may be low mounted position, or highly mounted wings, they may be elliptical, and it is a long list to be counted. There are some points that are related to wing aspects among them, all wings consist of spars, ribs, and skins, and all increase life forces by increasing their surfaces, which in turn lower the ability for maneuverability. In this work, two types of wing planforms will be studied, these are: tapered and swept-back wings, having different NACA models and two types of spars under the same aerodynamic and structural conditions to isolate the influence of planform geometry on natural frequencies, deflection patterns, and mode-shape coupling characteristics.

6 Wingspan calculations

In this study, two principal wing geometries were analyzed under the Aircraft overall weight is 1,100 kg, the speed is 50 m/s and $\rho = 1.225\ kg/m^3$ to isolate the effect of planform shape on overall span length. The configurations considered were:

a. Tapered wing
b. Swept back wing

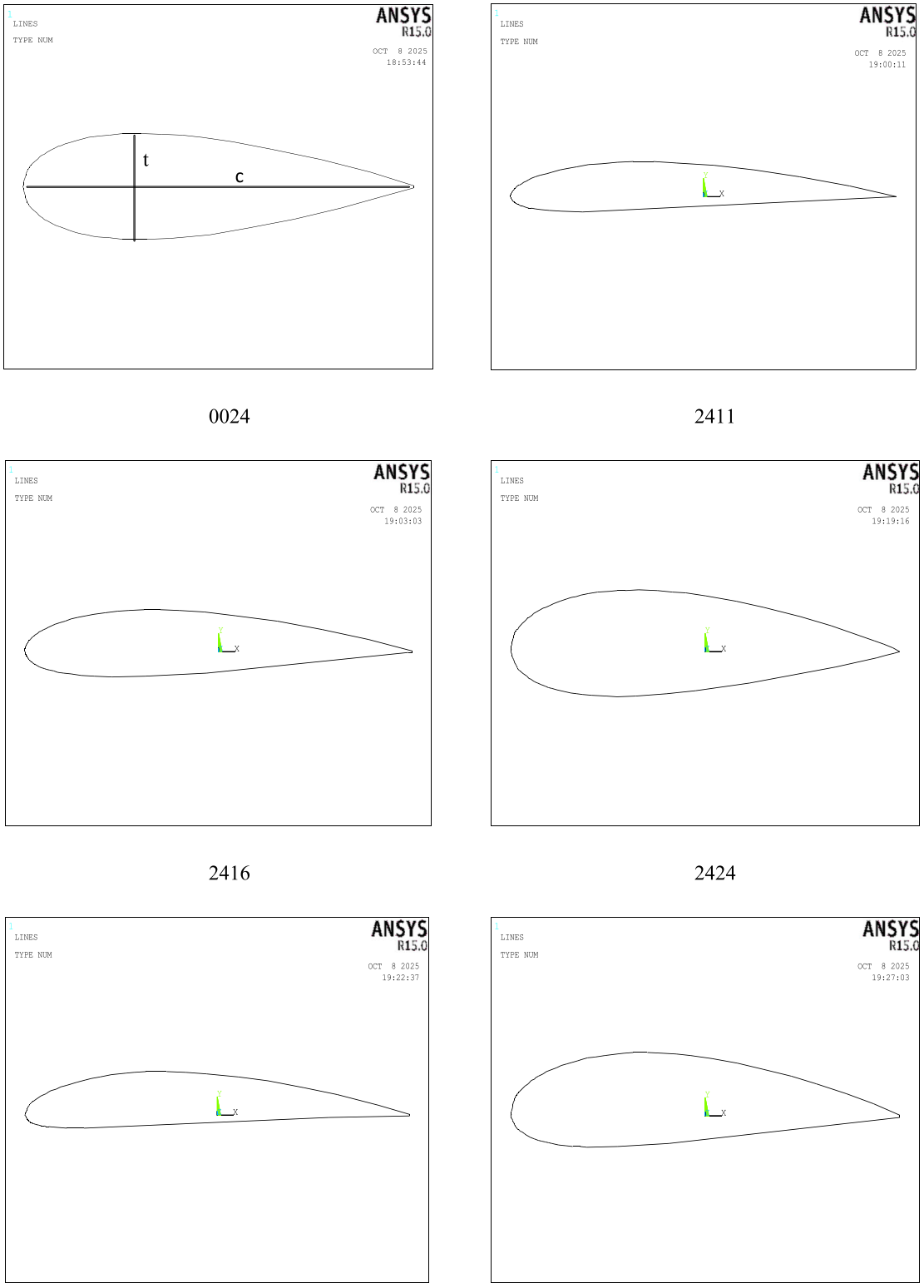

FIGURE 1
Geometrical characteristics of the studied NACA airfoils.

Each configuration was modeled for multiple NACA airfoil sections and evaluated at and spar section. The aerodynamic and geometric parameters were determined to ensure equivalent lift generation and structural loading across all cases (Mostakim et al., 2020).

6.1 Tapered wing

For the tapered wings, the principal geometric variable is the taper ratio (λ), defined in Equation 8 below, as:

TABLE 4 Box spar cross-section dimensions.

Width (cm)	Height (cm)	Thickness (mm)
8	8	5

$$\lambda = \frac{c_t}{c_r} \tag{8}$$

Where c_t and c_r are the tip and root chord lengths, respectively. The surface area was computed, and the corresponding span length was obtained from the projected planform area relation (Equation 9):

$$b = 2 \star \frac{S}{c_r\ (1+\lambda)} \tag{9}$$

Where, S is the surface area and b is the wing span. The calculated lift coefficients and surface areas for each NACA profile at a 9° which is acceptable for all the selected airfoils, are summarized in Table 2.

6.2 Swept back wing

For the swept-back configuration, a sweep angle of $\alpha_w = 30°$ was selected. The effective lift-curve slope for a swept wing can be expressed as presented in Equation 10 (Andreson, 2011):

$$a = \frac{a_0\, Cos\,(\alpha_w)}{1 + \sqrt{\left(\frac{a_0\, Cos\,(\alpha_w)}{\pi\, AR\, e}\right)^2 + \frac{a_0\, Cos\,(\alpha_w)}{\pi\, AR\, e}}} \tag{10}$$

Where a_0 is the two-dimensional airfoil lift slope, AR is the aspect ratio, and e is the Oswald efficiency factor and it is 0.95 (Mousa et al., 2022). The corresponding lift coefficients and wing dimensions are summarized in Table 3.

The results demonstrate that tapered wings generally exhibit larger span lengths and smaller surface areas for the same payload, indicating superior aerodynamic efficiency. In contrast, swept-back wings show reduced lift coefficients due to the effective decrease in aerodynamic loading caused by the sweep angle, though they offer improved stability and reduced drag at higher flight speeds. These findings establish the geometric foundation for the subsequent modal and vibration analyses performed using the FEM.

7 3D wing models representation

The three-dimensional wing geometries were generated in ANSYS Mechanical APDL (Release 15) using the aerodynamic parameters summarized in Tables 2, 3 for six selected four-digit NACA airfoil profiles. Each of the four digits has its own meaning. For example, NACA-2411 has a maximum distance between the cord line and the mean line of 2% of the cord length, and so-called camber or curvature localized at 4% of the cord length with a thickness to cord length ratio 11%. The airfoil section was defined by its x–y coordinate data, obtained from publicly available NACA databases in CSV format. The coordinates were imported into ANSYS and converted to key points, which were subsequently connected using spline curves to reconstruct the exact airfoil contour, as illustrated in Figure 1.

The resulting two-dimensional profiles were extruded along the spanwise direction to generate the wing skin with a uniform thickness of 1.6 mm and a taper ratio of 0.4. To simulate the internal structural framework, ribs must be spaced according to some reliable standard, and it is documented that rib spacing could achieve a good balance between weight and wing strength if it is around 25%–50% of the wing cord length (Arunkumar et al., 2012). Eleven equally spaced ribs were introduced for both tapered and swept configurations. Each wing was reinforced by either a box spar or an I-section spar, whose geometric properties are listed in Tables 4, 5, respectively.

ANSYS Parametric Design Language (APDL) script was developed to automate the construction of 3-D wing models. The script sequentially defined airfoil coordinates, spline surfaces, ribs, and spars, and then extruded and mirrored the geometry to form the full wing structure. Table 6 lists the sequential input and processing steps to build up 3-D NACA wing geometry.

The use of step-by-step programming in ANSYS numerical analyzer environment offers several advantages: all models are represented in a consistent manner, eliminating variations due to approximation or human error, and ensuring faster execution. Sample results from using the program are shown in Figures 2–4.

8 Finite element analysis

Among the most well-known experimental research techniques for measuring wing performance and flexibility is structural or Ground Vibration Testing (GVT), which addresses structural aspects, and wind tunnel tests to evaluate aerodynamic performance. The accuracy of these methods is subject to several limitations and challenges, including high cost, the need for time recording and preparation, and, most importantly, the requirement to take the aircraft out of service for the research, in addition to numerous human factors. The FEM overcomes these problems with an acceptable approach, a small margin of error, and the ability to study a wide range of engineering aspects (Mousa et al., 2022). In the present study, FEM was used to determine the natural frequencies and mode shapes of various wing geometries in order to assess the influence of planform and spar configuration on vibration characteristics.

TABLE 5 I section spar dimensions.

Width (cm)	Height (cm)	Web thickness (mm)	Flange thickness (mm)
8	8	5	5

TABLE 6 Excerpt from the APDL code for tapered NACA 2411 wing (box spar).

Page No. 1	Page No. 2
/BATCH	BSPLIN, ,P51X
! /COM,ANSYS RELEASE 15.0.7 UP20140420 17:55:25 08/25/2025	LSTR, 59, 1
/input,start150,ans,'C:\Program Files\ANSYS Inc\v150\ANSYS\apdl\'	FLST,3,3,4,ORDE,2
!*	FITEM,3,1
/PREP7	FITEM,3,-3
k , , 100 , 0.001 , ,	LGEN, ,P51X, , ,-50, , , ,1
k , , 99.73 , 0.059 , ,	FLST,2,3,4
k , , 98.918 , 0.235 , ,	FITEM,2,2
k , , 97.578 , 0.52 , ,	FITEM,2,1
k , , 95.72 , 0.906 , ,	FITEM,2,3
k , , 93.365 , 1.38 , ,	AL,P51X
k , , 90.535 , 1.927 , ,	FLST,2,1,5,ORDE,1
k , , 87.26 , 2.532 , ,	FITEM,2,1
k , , 83.577 , 3.175 , ,	ARSCALE,P51X, , ,,97,0.97,1, ,0,0
k , , 79.52 , 3.839 , ,	FLST,2,2,5,ORDE,2
k , , 75.138 , 4.506 , ,	FITEM,2,1
k , , 70.475 , 5.158 , ,	FITEM,2,-2
k , , 65.583 , 5.777 , ,	VEXT,P51X, , ,196,0,-340,0.4,0.4,,
k , , 60.513 , 6.347 , ,	FLST,3,2,6,ORDE,2
k , , 55.322 , 6.852 , ,	FITEM,3,1
k , , 50.067 , 7.276 , ,	FITEM,3,-2
k , , 44.807 , 7.606 , ,	VGEN,2,P51X, , ,200, , , ,0
k , , 39.597 , 7.83 , ,	VDELE, 1, , ,1
k , , 34.455 , 7.912 , ,	!KDIST, 39, 42
k , , 29.485 , 7.831 , ,	VSBV, 3, 4
k , , 24.745 , 7.588 , ,	BLOCK,-75,375,-40,40,-2,-338/10,
k , , 20.292 , 7.193 , ,	FLST,3,1,6,ORDE,1
k , , 16.175 , 6.659 , ,	FITEM,3,3
k , , 12.448 , 6.006 , ,	VGEN,10,P51X, , , , ,-338/10, ,0
k , , 9.148 , 5.253 , ,	!KDIST, 124, 42
k , , 6.317 , 4.427 , ,	FLST,3,10,6,ORDE,2
k , , 3.985 , 3.553 , ,	FITEM,3,3
k , , 2.17 , 2.654 , ,	FITEM,3,-12
k , , 0.897 , 1.752 , ,	VSBV, 2,P51X
k , , 0.172 , 0.862 , ,	FITEM,3,1
k , , 0 , 0 , ,	FLST,3,1,6,ORDE,1
k , , 0.375 , -0.794 , ,	FITEM,3,1
k , , 1.29 , -1.483 , ,	VGEN, ,P51X, , ,-200, , , , ,1
k , , 2.723 , -2.061 , ,	RECTNG,-4,4,-4,4,
k , , 4.662 , -2.531 , ,	RECTNG,-3.5,3.5,-3.5,3.5,
k , , 7.08 , -2.893 , ,	ASBA, 4, 5
k , , 9.948 , -3.151 , ,	FLST,3,1,5,ORDE,1
k , , 13.238 , -3.31 , ,	FITEM,3,6
k , , 16.912 , -3.379 , ,	AGEN, ,P51X, , ,-25,2 ,5 , , ,1
k , , 20.932 , -3.368 , ,	FLST,2,1,5,ORDE,1
k , , 25.255 , -3.291 , ,	FITEM,2,6
k , , 29.842 , -3.165 , ,	VEXT,P51X, , ,196,0,-344,0.4,0.4,,
k , , 34.642 , -3.005 , ,	FLST,2,13,6,ORDE,4
k , , 39.612 , -2.83 , ,	FITEM,2,1
k , , 44.74 , -2.637 , ,	FITEM,2,-2
k , , 49.933 , -2.415 , ,	FITEM,2,13
k , , 55.132 , -2.174 , ,	FITEM,2,-23
k , , 60.28 , -1.925 , ,	VADD,P51X
k , , 65.32 , -1.677 , ,	FLST,2,1,6,ORDE,1
k , , 70.198 , -1.436 , ,	FITEM,2,3
k , , 74.862 , -1.208 , ,	VLSCAL,P51X, , ,1/100,1/100,1/100, ,0,1
k , , 79.257 , -0.994 , ,	!LGWRITE,'wwww','lgw','C:\Users\NS\Desktop\', COMMENT
k , , 83.337 , -0.798 , ,	

The most in use material in aircraft manufacturing sectors is aluminum alloys due to the superior strength to weight ratio. Aluminum mechanical properties and its behavior are subjected to different tests in order to be carefully fit analytically. Results and previous works documented that aluminum use in airplane industry and their simulations are matched under linear elastic material assumptions.

The behavior of aluminum alloys used in aircraft vibration modeling is treated as linearly elastic, isotropic, and homogeneous. The rationale behind these assumptions is that the aircraft is designed to operate without plastic deformation, which is itself a cause of wing failure, and that its properties are sufficiently uniform to be considered practically isotropic and homogeneous. Experiments have shown that the margin of error resulting from these assumptions is small (between 1% and 5%), and they can be relied upon, especially for research purposes, without the need for complex nonlinear models (Doğan and Şahin, 2021).

Each wing model consists of three major structural components, skin, ribs, and spars, constructed from aluminum alloys commonly used in aircraft structures. The material properties of these components are listed in Table 7. All materials were modeled as linear elastic and isotropic, an assumption that is valid for the small-deformation regime considered in this analysis (He et al., 2023).

All models were discretized using SOLID186, a 20-node hexahedral (brick) element capable of modeling irregular geometries and supporting both structural and coupled-field analyses. SOLID186 elements are well-suited for modeling aerospace structures, gear drives, metallic frameworks, and thermal–structural problems due to their ability to handle both linear and nonlinear material behavior as well as contact interactions. Each node in this element has three translational degrees of freedom (in the x, y, and z directions), resulting in a total of 60 degrees of freedom per element. In general, the rounding and discretization errors are the two main errors encountered with the choice of element type so that it must be obeyed a certain procedure to avoid such errors. Many elements are adequate to fit the problem and reach the solution but with different accuracies like quad, brick and tetrahedral elements. Here, brick elements are adopted to simulate the natural frequency. The right element number will be chosen according to the convergence test to achieve good balance between the discretization and round-off errors by increasing the number of elements gradually till it reaches 14,000 elements; to confirm the results of previous work as it will be discussed in verification subject. The geometry of the brick element is illustrated, and the fully discretized 3-D finite element model, in addition to the FEM solution flowchart, is shown in Figure 5.

9 Results and discussions

9.1 Modal behavior of box-spar wings

The results in Figure 6 illustrate the effect of the synergy of the different wing parts on their natural frequency and the amount of deflection in the 6th mode.

Figures 7, 8 present the variation of deflection and natural frequency for the three structural configurations (spar only, spar with ribs, and complete wing structure) across the first six vibration modes. The results clearly indicate that the addition of ribs and skin significantly enhances the structural stiffness of the wing. The maximum deflection decreases by approximately 80% when progressing from the isolated spar to the fully assembled wing

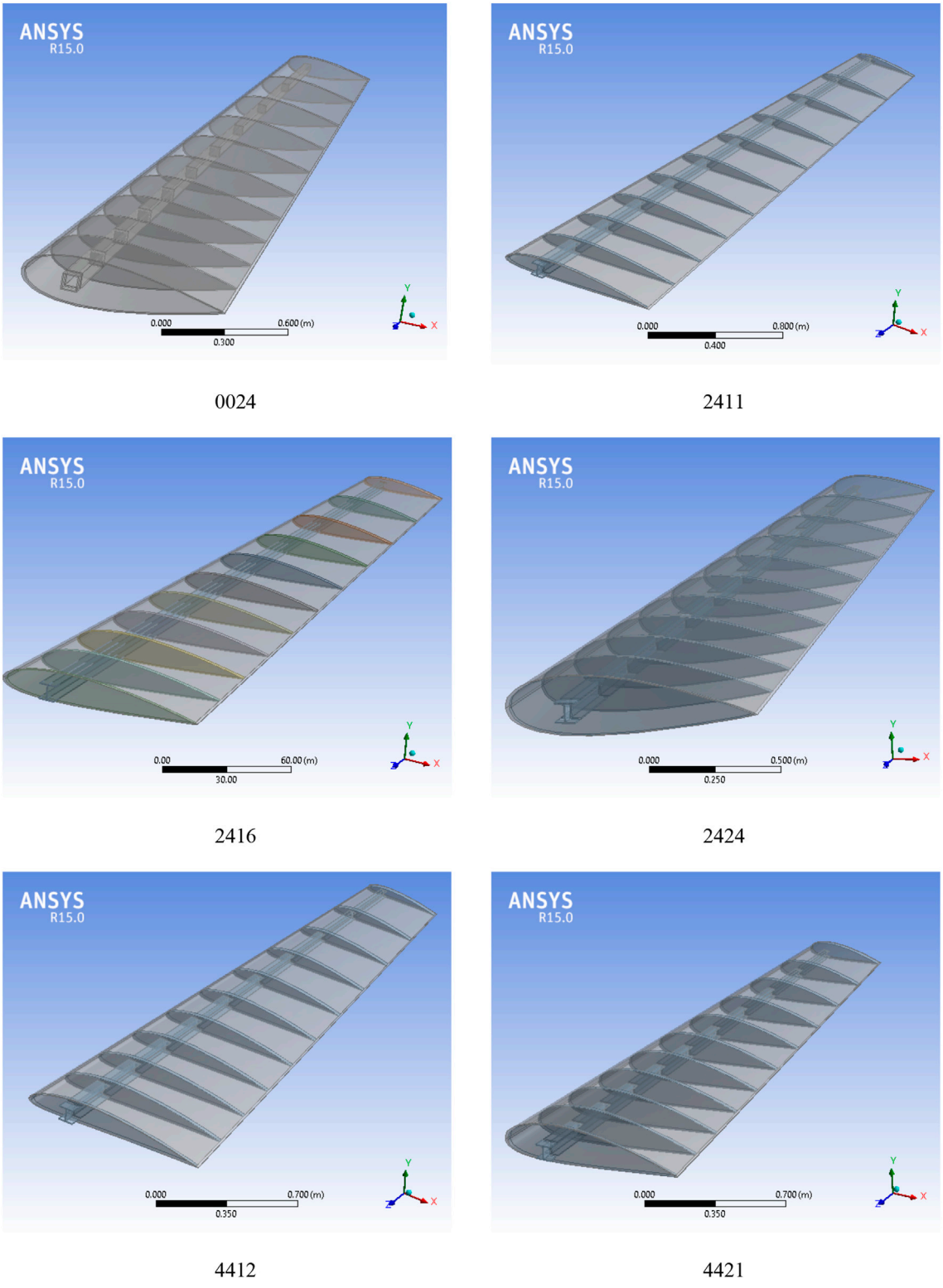

FIGURE 2
Samples of different 3-D wings models.

structure. Correspondingly, the natural frequencies increase by about 120%, demonstrating the direct correlation between stiffness enhancement and vibrational performance. This improvement arises from the synergistic contribution of the ribs and skin, which distribute aerodynamic and inertial loads more uniformly and increase the wing's resistance to bending and torsion.

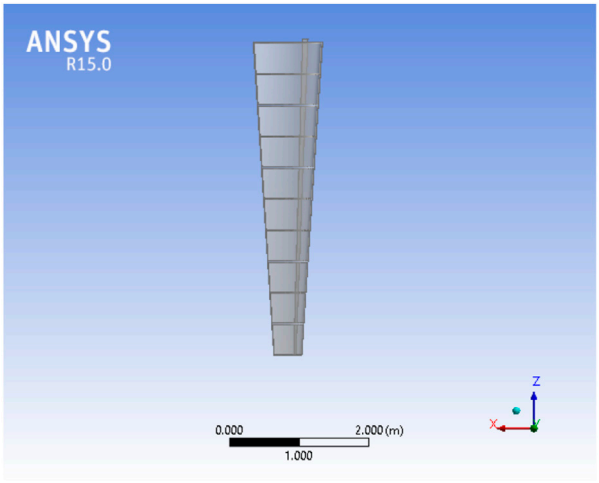

FIGURE 3
Taper wing layouts.

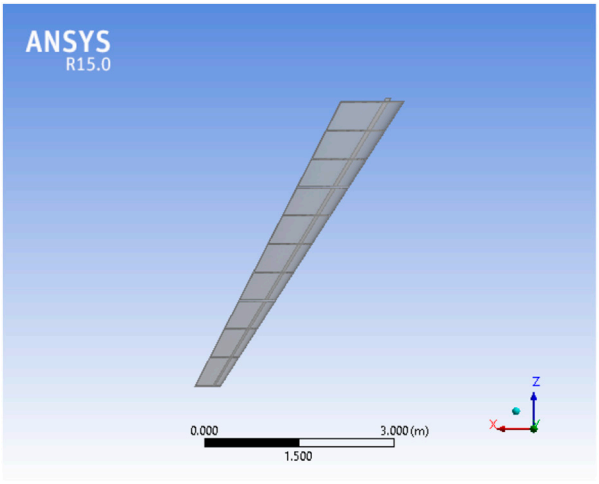

FIGURE 4
Swept wing layout.

The box-spar wing configuration for the NACA 0024 profile was analyzed to obtain six natural modes within the frequency range of 6.55–110.8 Hz. (Figures 9–14), illustrate samples of FE solutions for the deformation patterns associated with the first six vibration modes of box spar NACA 0024 tapered wing. The first two modes Figures 9, 10 are bending-dominated, exhibiting maximum deflection at the wing tip, while the intermediate modes (Figures 11–13) show clear bending–torsion coupling, particularly evident in the fourth and fifth modes. The 6th mode, is set up at 110.8 Hz, encountered horizontal bending mode as in Figure 14.

These results confirm that the closed-cell box-spar structure provides enhanced global stiffness and effectively suppresses torsional deformation, maintaining structural integrity even in higher-order bending modes. This behavior aligns with previous findings by (Sedaghati et al., 2006; Viglietti et al., 2017), who demonstrated that box-spar wings achieve superior stiffness and higher modal frequencies compared with open-section spars.

9.2 Modal behavior of I-Section spar wing

The I-section spar configuration exhibits relatively lower structural stiffness, with corresponding natural frequencies ranging from 4.69 to 111.78 Hz. Figures 15–20 illustrate samples of FE solutions for the deformation patterns associated with the first six vibration modes of I spar NACA 0024 tapered wing. The first mode (Figure 15) primarily represents horizontal bending about the lateral (y) axis, while the second mode (Figure 16) corresponds to vertical bending about the horizontal (x) axis. Figures 17–19 show the complex bending–coupled torsion modes, with maximum effects at wing mid span and wing tip. Higher bending mode is shown in Figure 20, it is noticeable that such mode encountered with high frequency due to the high sectional impedance against deflection in that direction. It is the same behavior of the same sequence having I section spar but with higher deformation. I section spars are of reduced torsional rigidity, so that their deformation is higher in comparison with those of box spars but with lower frequencies. The average difference in natural frequencies is about 9.5%–22%. This result is consistent with the analytical and experimental findings reported by (Demirtaş and Bayraktar, 2019), who analyzed a NACA 4415 airfoil wing modeled as a cantilever beam using both theoretical and FEM approaches in ANSYS, reporting fundamental frequencies between 4.3 Hz and 365.3 Hz with deviations of approximately 1.3%–11.9% between theoretical and numerical results, confirming that simplified FEM beam representations can accurately predict modal trends in aircraft wings.

TABLE 7 Different wing parts mechanical properties, Aluminum alloys.

No.	Part	Material	Modulus of elasticity (GPa)	Poisson's ratio	Density (kg/m^3)	Thickness (mm)	Tensile strength, MPa, min.	Yield strength (0.2% offset), MPa, min.	Elongation, %, min.
1	Spars	7075-T6	71.7	0.33	2810	5	540.0	485	7.0
2	Ribs	2024-T3	73	0.33	2780	5	435.0	290.0	15.0
3	Skin	2024- T3	73	0.33	2780	1.6	435.0	290.0	15.0

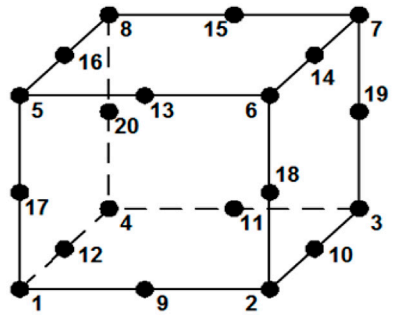

a

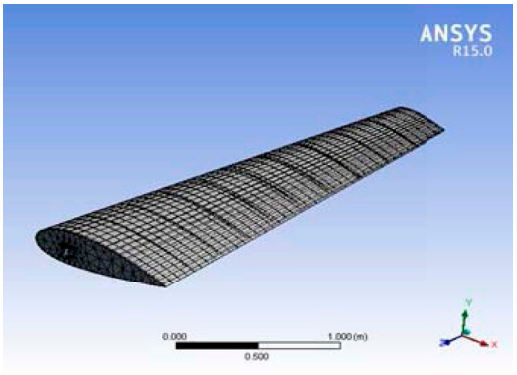

b

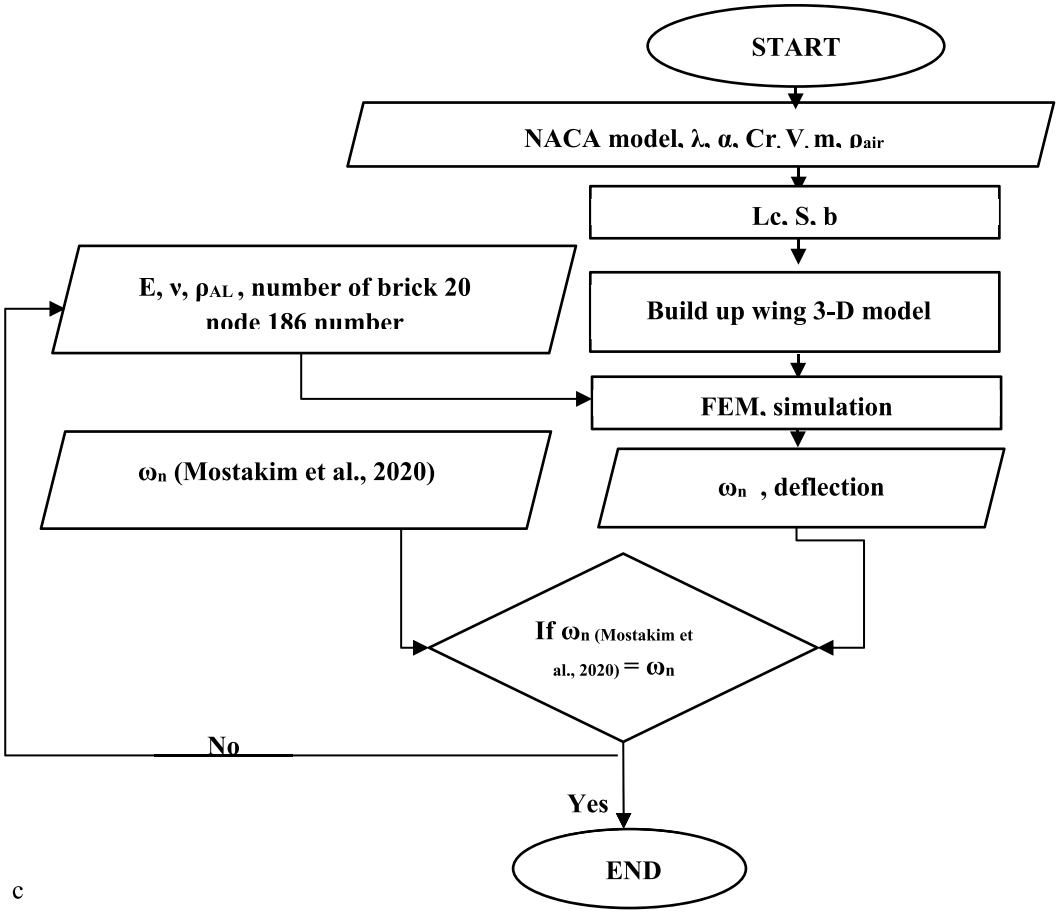

c

FIGURE 5
FE solution details; element type layout, discretized wing model and flowchart. **(a)** Solid brick element 20 node 186. **(b)** FE model, brick element discretization. **(c)** Solution flowchart.

9.3 Modal frequencies for different wing geometries

The natural frequencies obtained for the six NACA profiles under both box-spar and I-section configurations are illustrated in Figures 21–24, showing the modal frequency progression for tapered and swept-back wings, respectively. Across all configurations, the natural frequency increases progressively with mode number, indicating enhanced structural stiffness and the activation of higher-order bending and torsional responses. The results clearly reveal that box-spar wings exhibit 9.5%–22% higher natural frequencies compared to their I-section counterparts across all modes.

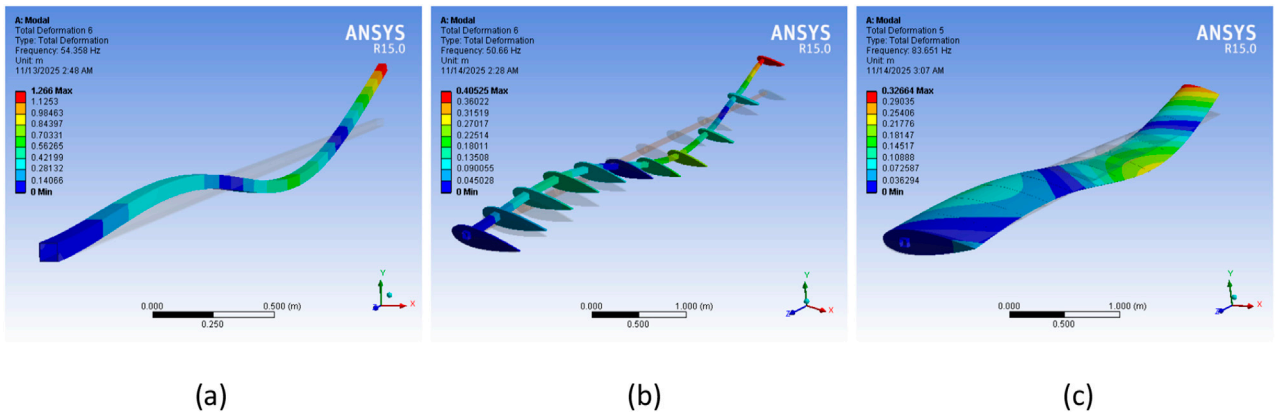

FIGURE 6
Effect of wing element assembly on natural frequency and deflection for 6th mode, **(a)** spar only, **(b)** spar and ribs, **(c)** whole wing structure.

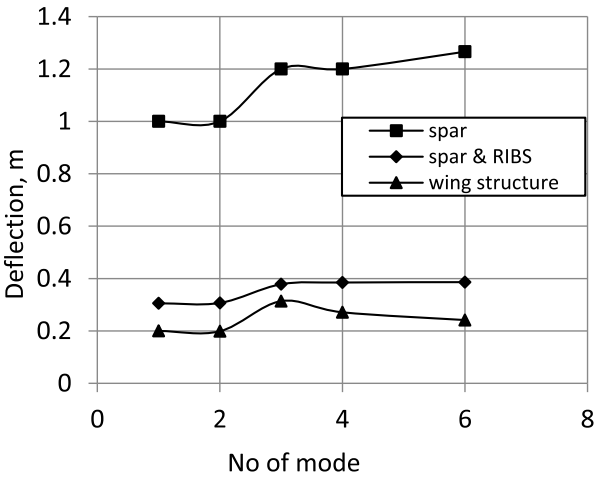

FIGURE 7
Deflection of spar, spar and ribs and wing structure.

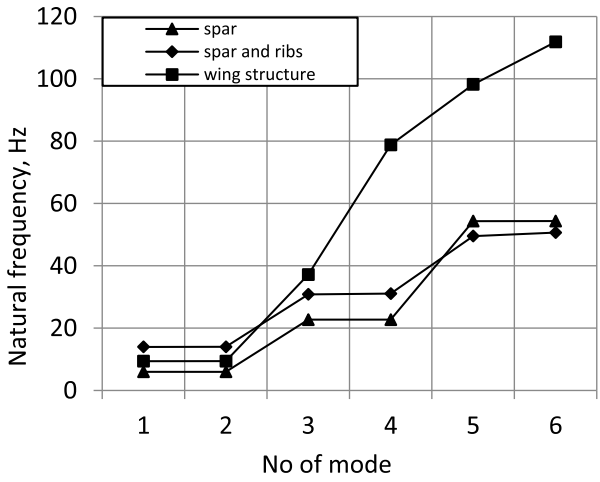

FIGURE 8
ω_n of spar, spar and ribs and wing structure.

Such increase could be attributed to the high torsional rigidity of box spar section which increases the ability to absorb dynamic loading energy. In the other hand I- section appear to have lower natural frequencies because of their lower torsional rigidity.

Thicker wing sections; NACA 0024 and NACA 2424, showed higher natural frequencies due to their higher stiffness resulted from the higher 2nd moment of area. Such thicker profiles increase bending stiffness and shift the coupling between bending and torsion modes. Camber effect: from results of NACA- 0024 and NACA- 2424, it is clear that as large camber value is as larger as natural frequency and that because curvature gives more strength to section and in turn higher stiffness. The increase could be about 70%. Comparing NACA- 2424, 2416 and 2424, eliminate the effect of camber and spot the light on wing thickness, results show that increasing wing thickness could increase stiffness and in turn the resulted frequencies which increase by about 55% for thicker sections. Overall view on natural frequency results shows that; always taper wings natural frequencies are higher than swept wings with 22% for box spar and 9.5% for I- section spar. It has been found that the effect of spar results is reduced in case of adopting swept wings; it could be about 13% greater than that of I- section in case of taper wings. The combined effect of using spar type and wing plan could reach 20% in case of using I- spar swept wing, all assessment is referenced to the box- spar taper wing. From Figure 21 for tapered - box spar wing the mean neutral frequents at 1st mode is 9.75 Hz, while for swept back–I spar wing in Figure 24 the mean neutral frequents at 1st mode is 7.3 Hz, and that reflect the higher overall stiffness.

Finally, results emphasis the domination of geometrical role on altering the natural frequency of the wing due to their effects on stiffness and compliance, I spar- swept has lower stiffness compared to that of box- spar taper wings. These numerical observations are consistent with the global trends summarized in the Abstract and

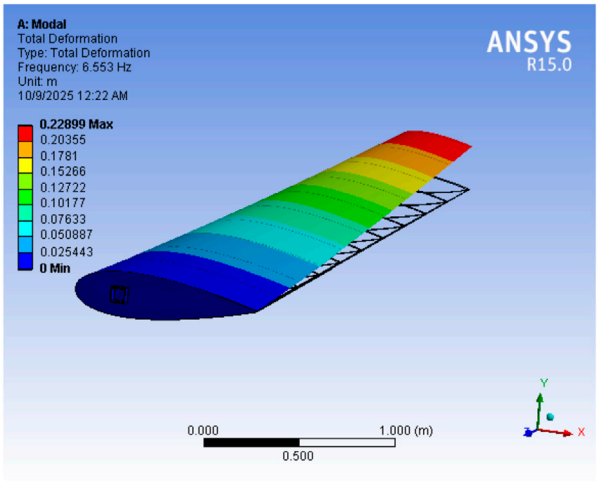

FIGURE 9
0024 1st mode ω_n and deflection (bending).

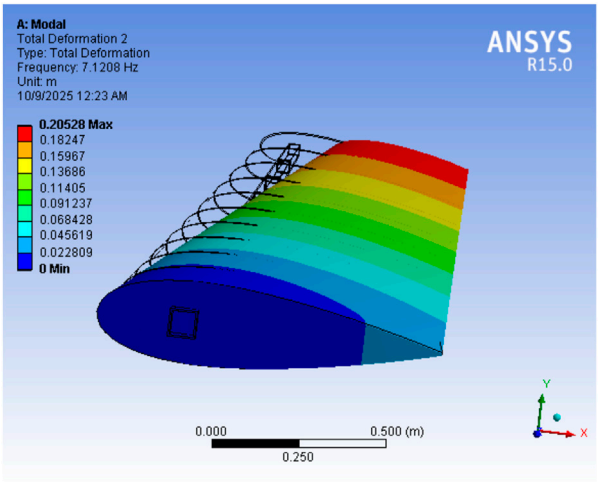

FIGURE 10
0024 2nd mode ω_n and deflection (bending).

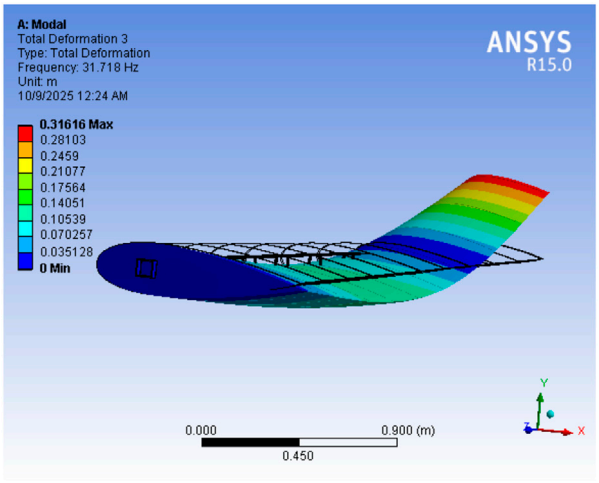

FIGURE 11
0024 3rd mode ω_n and deflection, box spar (couple of bending and torsion).

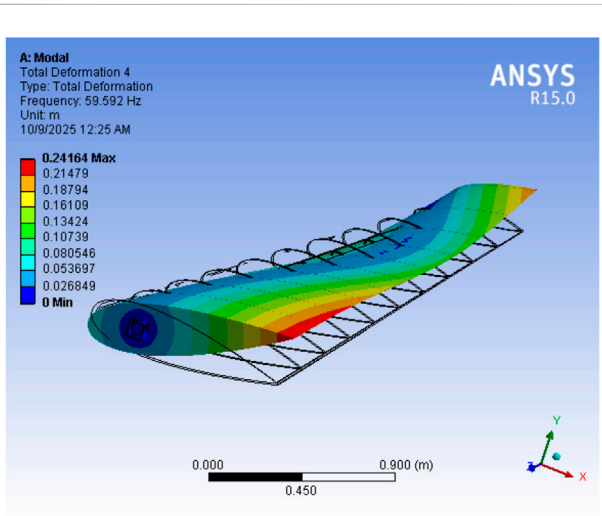

FIGURE 12
0024 4th mode ω_n and deflection, box spar (couple of bending and torsion).

Conclusions, aligning with previously reported aeroelastic studies (Pagani et al., 2014; Viglietti et al., 2017; Patuelli et al., 2023).

9.4 Deflection characteristics

Figures 25–28 illustrate the variation of modal deflection amplitudes for the four principal wing configurations, tapered box-spar, tapered I-section, swept box-spar, and swept I-section, across the six analyzed NACA airfoil profiles. Deflection amplitudes increase progressively with mode number for all configurations, corresponding to the higher strain energy and localized deformation associated with higher-order modes. Lower modes are dominated by bending, while higher modes exhibit pronounced bending–torsion coupling, particularly near the wing tip. Across all geometries, box-spar wings display 20%–30% greater deflection magnitudes than I-section wings, indicating higher compliance under dynamic excitation. Introducing I- section spar plays a positive role regarding the maximum deflection value and its distribution along wing span due to its effect on beam stiffness especially at higher modes. NACA- 4412 is largely deflected because of its thin profile, for both types of spars, while NACA- 0024 and 2424 exhibit the smallest deflection especially those with I sections, reaffirming the superior stiffness of thick sections. Planform effect on deflection became more evident at higher frequencies; swept wings have 25% higher deflection than that of taper wings in case of I spar and 14% for box spar at 6th mode. I- section spar taper wings are firstly ranked regarding vibration characteristics and their small deflection while the last in ranked wing arrangement is the swept back one with box spar.

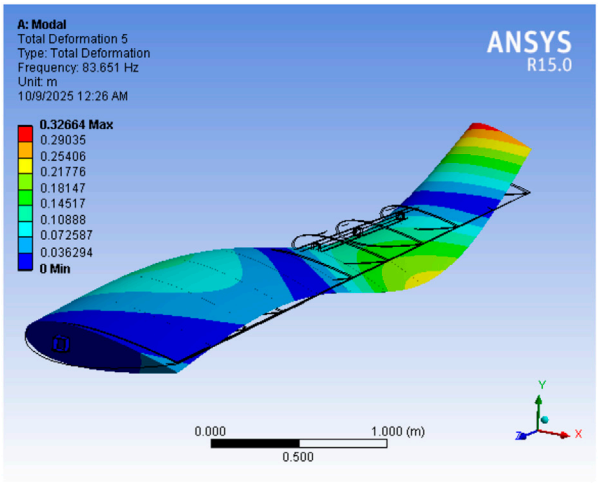

FIGURE 13
0024 5th mode ω_n and deflection, box spar (couple of bending and torsion).

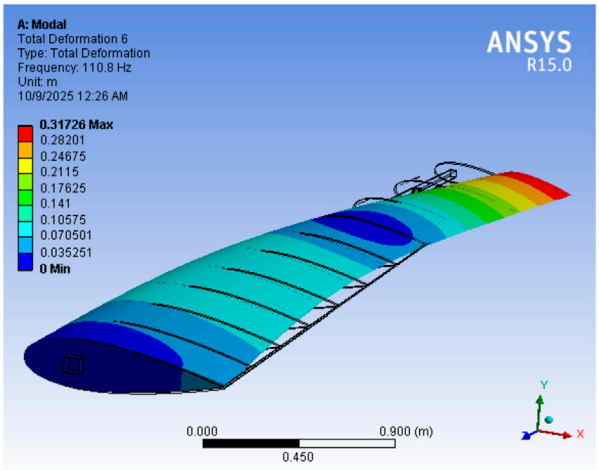

FIGURE 14
0024 6th mode ω_n and deflection, box spar (bending).

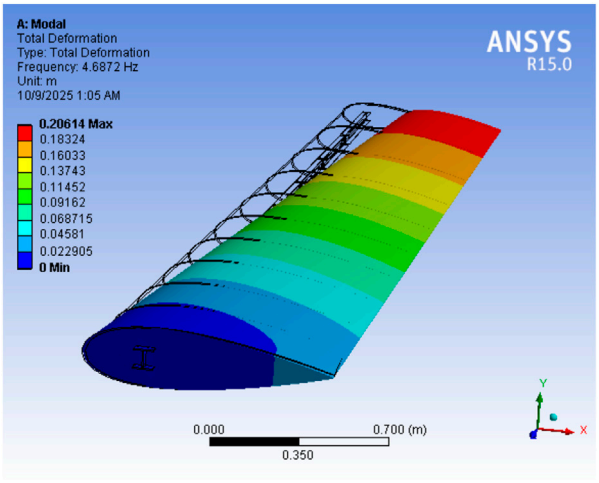

FIGURE 15
0024 1st mode ω_n and deflection, I section (bending).

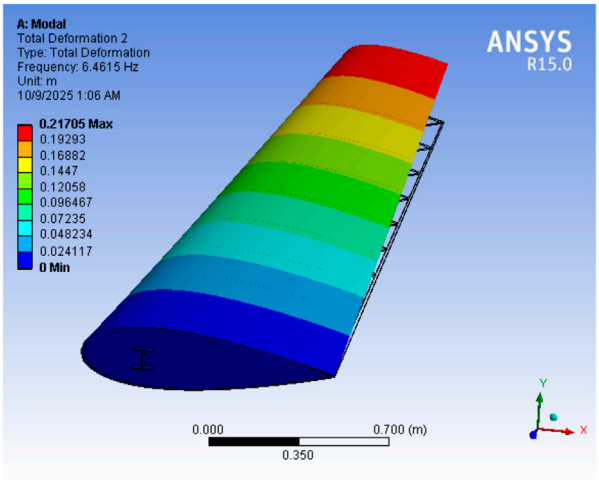

FIGURE 16
0024 2nd mode ω_n and deflection, I section (bending).

Overall, these results are bridged between aerodynamic efficiency and structural rigidity, in line with earlier finite element and experimental analyses. According to FEM and experimental investigations (Viglietti et al., 2017; Demirtaş and Bayraktar, 2019; Patuelli et al., 2023).

9.5 Statistical analysis and overall comparative discussion

To quantitatively assess the effect of wing shape and spar configuration on vibration, a two-way Analysis of Variance (ANOVA) was performed. The independent variables were wing shape (pointed vs. slanted) and spar cross-section (box vs. I-section), and the dependent variables were the normal frequency and deformation of the six NACA wings. ANOVA breaks down the total difference in results into components attributable to each element and its interaction, allowing for an objective assessment of their relative influence on the response variables. The F-value represents the ratio of the group mean to the intragroup variance and is expressed in Equation 11 as follows:

$$F = \frac{MS_{between}}{MS_{within}} \tag{11}$$

Where MS between and MS within denote the mean square values for between-group and within-group variations, respectively. A higher F-value indicates a stronger influence of the tested factor. The p-value corresponds to the probability that the observed differences occurred by random chance; results are significant within p-value less than 0.05. Table 8 summarizes the ANOVA results for both natural

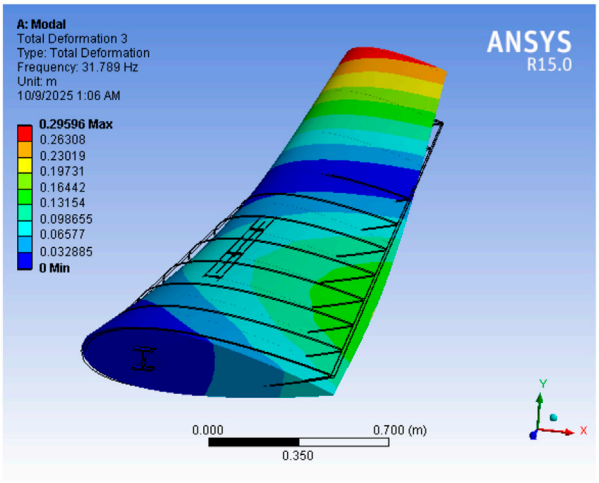

FIGURE 17
0024 3rd mode ω_n and deflection, I section (couple of bending and torsion).

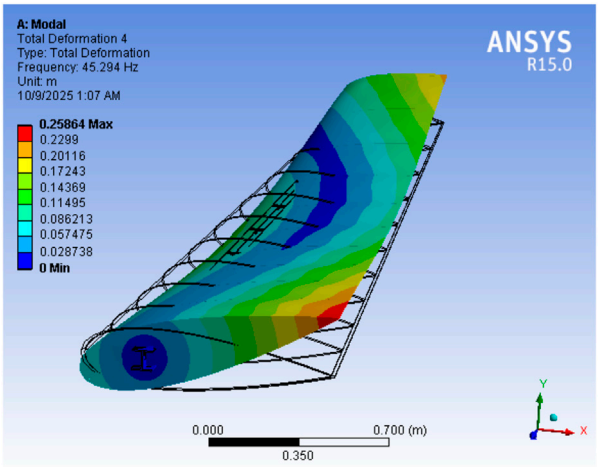

FIGURE 18
0024 4th mode ω_n and deflection, I section (couple of bending and torsion).

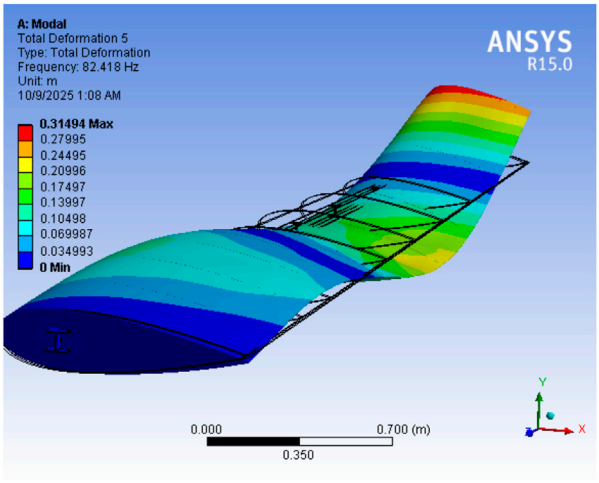

FIGURE 19
0024 5th mode ω_n and deflection, I section (couple of bending and torsion).

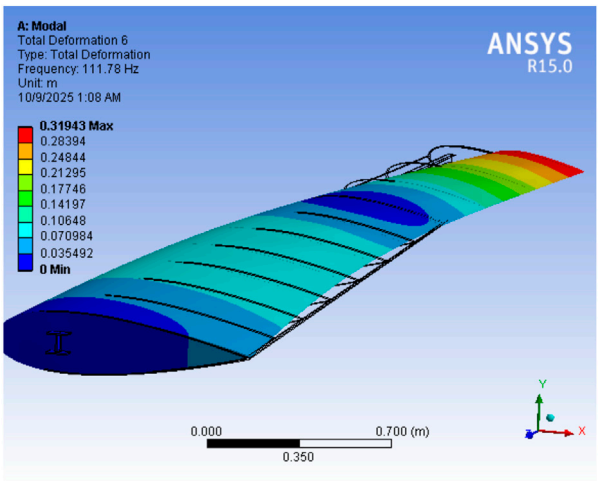

FIGURE 20
0024 6th mode ω_n and deflection, I section (bending).

frequencies and deflection amplitudes. The data indicate that wing geometry has a more pronounced influence on the vibrational characteristics than spar configuration. Although the p-values slightly exceed the conventional 0.05 threshold, the consistent directional trends across all modes confirm the mechanical (rather than purely statistical) significance of the observed variations. Specifically, tapered wings achieved higher modal frequencies than swept-back configurations, primarily due to their shorter effective spans and enhanced chordwise stiffness distribution. Box-spar models exhibited greater torsional rigidity and bending resistance, with natural frequencies on average 9.5%–22% higher than those of I-section spars.

For the deflection amplitudes, similar tendencies were observed. Tapered I-spar wings demonstrated the lowest deflection levels, approximately 20%–30% lower than swept or box-spar configurations, reflecting superior bending rigidity and load-bearing performance. Conversely, swept-back wings exhibited greater deflection amplitudes, indicating increased compliance under dynamic excitation. Among the airfoil profiles, NACA 4412 showed slightly higher deformation levels owing to its thinner cambered section, which reduces torsional rigidity despite aerodynamic advantages. The inclusion of the ANOVA summary (Table 8) demonstrates that, although the differences are not statistically significant at the 95% confidence level, they are systematic, repeatable, and physically consistent across all configurations studied. These results confirm that tapered wings with I-section spars provide the most efficient balance between stiffness and structural weight. The mechanical consistency of the

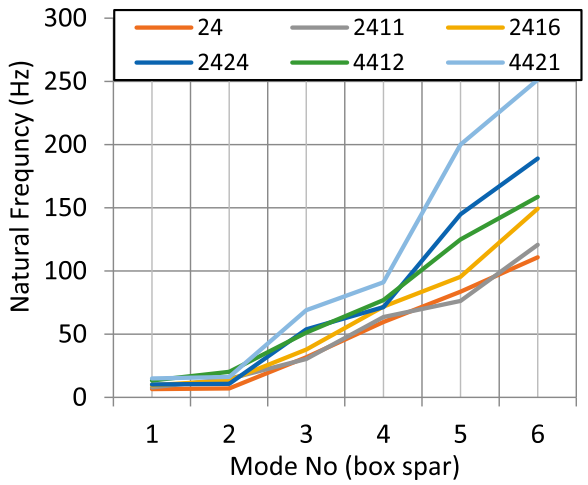

FIGURE 21
Variation of natural frequency for taper wings (box-spar configuration).

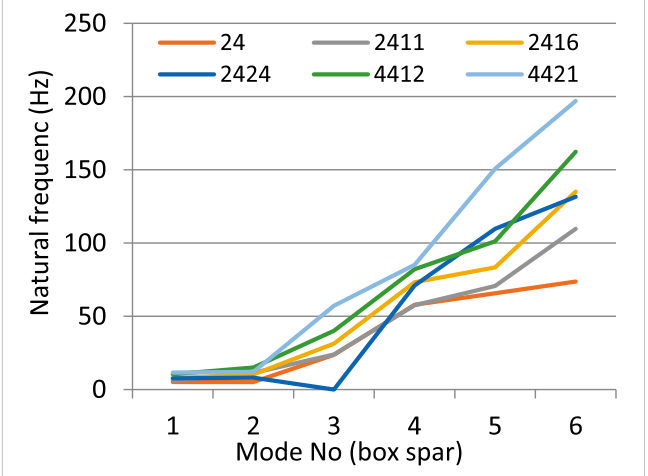

FIGURE 23
Variation of natural frequency for Swept-back wings (box-spar configuration).

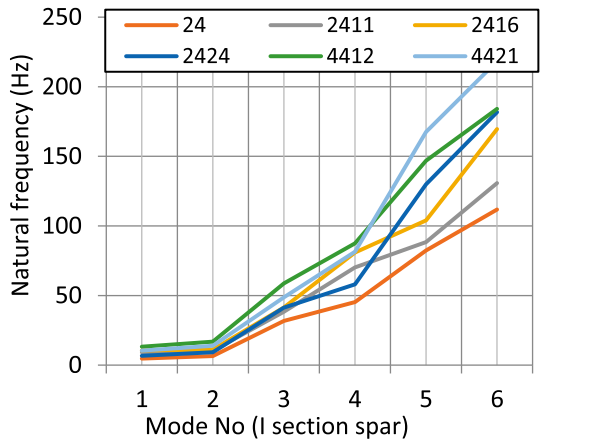

FIGURE 22
Variation of natural frequency for taper wing (I-section configuration).

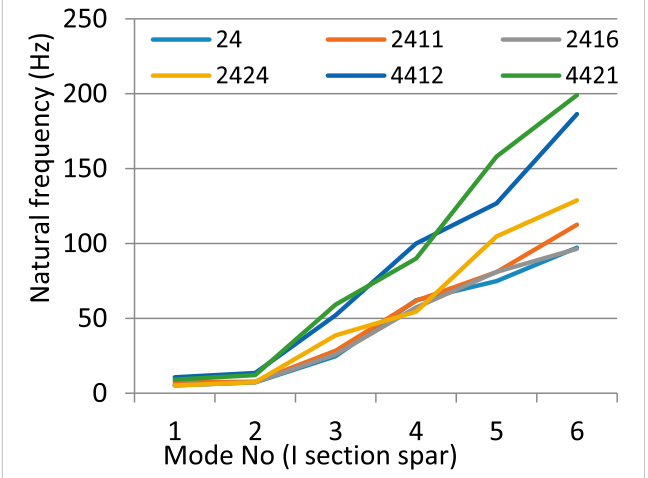

FIGURE 24
Variation of natural frequency for Swept-back wings (I-section configuration).

findings reinforces the reliability of the finite element predictions and establishes a solid basis for future experimental and aeroelastic validation studies (Guo et al., 2006; Jonsson et al., 2023; He et al., 2023).

9.6 Verification for the results

Ensuring the accuracy of the 3D model representation, setting its boundary conditions, and considering its material behavior assumptions in FEM environment lends reliability to the results and conclusions. The current work shares some similarities with previous studies, such as materials and type of analysis, but differs in the wing models, studied variables and scope. Mostakim et al. (2020) investigates the natural frequency using the FEM for a rectangular, solid aluminum wing. The studied wing section was NACA 4412; its dimensions are listed in Table 9. The wing was modeled and its vibration analyzed, the results were consistent, as shown in Figures 29, 30. Results show that the discrepancy of 1st mode frequency from that of (Mostakim et al., 2020) is 0.2% and 0.4%.

9.7 Practical implications and nonlinear considerations

The findings of this study carry significant practical implications for the structural design and optimization of modern aircraft wings, particularly regarding vibration

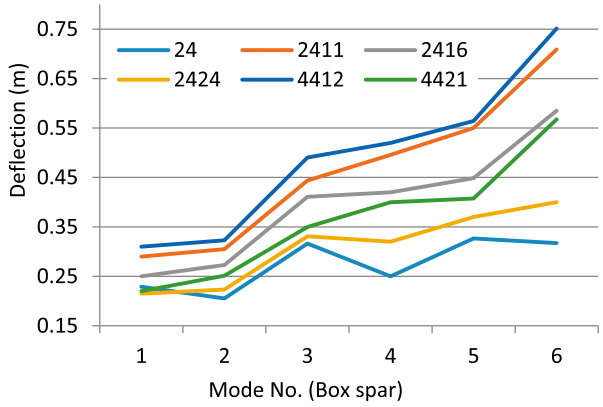

FIGURE 25
Deflection vs. mode number for taper wings (box-spar configuration).

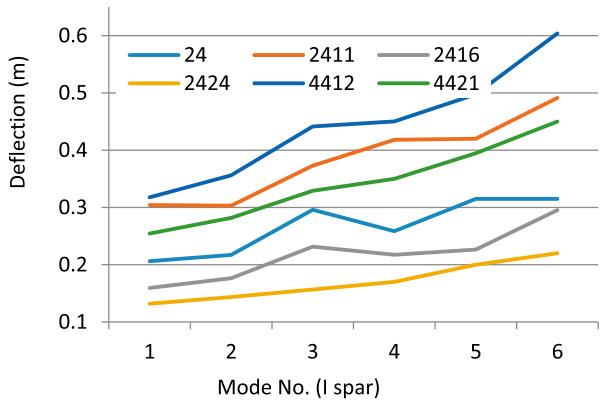

FIGURE 26
Deflection vs. mode number for taper wing (I-section configuration).

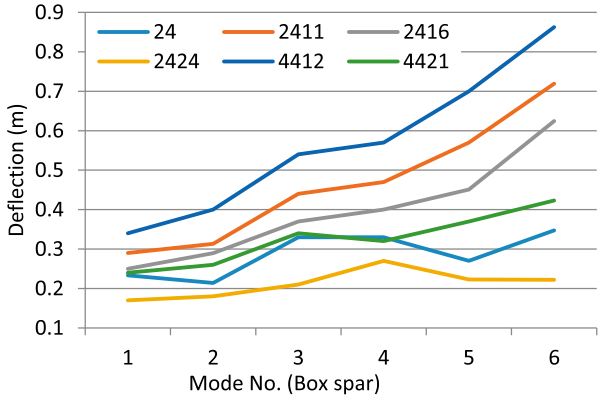

FIGURE 27
Deflection vs. mode number for Swept-back wings (box-spar configuration).

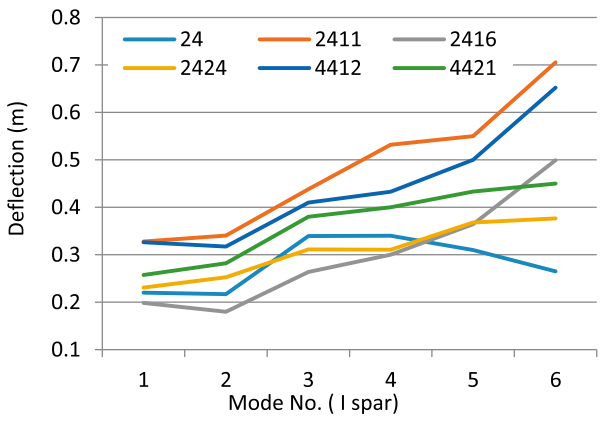

FIGURE 28
Deflection vs. mode number for Swept-back wings (I-section configuration).

control and aeroelastic stability. The demonstrated sensitivity of natural frequencies and deflection characteristics to both wing geometry and spar configuration provides valuable guidance for early-stage wing design. Specifically, the higher modal frequencies observed in tapered I-section wings suggest improved resistance to aeroelastic instabilities such as flutter and divergence, making them suitable for medium-payload and Unmanned Aerial Vehicles (UAVs) operating under variable aerodynamic loads. Conversely, the greater compliance of swept box-spar wings may be advantageous in applications requiring enhanced energy absorption or structural flexibility, such as morphing or deployable wing systems. These insights confirm that structural tailoring through the careful selection of spar topology and airfoil thickness can effectively balance stiffness, weight, and vibration performance in practical aerospace structures.

It is important to note that the present analysis is based on linear elastic assumptions, neglecting both material and geometric nonlinearities. In realistic flight conditions, nonlinear effects can significantly alter the dynamic behavior of flexible wings. Geometric nonlinearity arising from large deflections may cause stiffness softening or hardening, resulting in frequency shifts or mode coupling, while material nonlinearity under high stress or fatigue loading could lead to local yielding or viscoelastic damping. Additionally, aeroelastic coupling between aerodynamic forces and structural deformation may amplify or suppress modal responses depending on flight conditions, potentially affecting flutter margins and overall dynamic stability.

To evaluate these complex interactions more accurately, future work should integrate nonlinear finite element formulations with Computational Fluid Dynamics (CFD) to perform fully coupled fluid–structure interaction (FSI) analyses. This approach would enable the prediction of post-critical behavior, flutter onset, and dynamic stability under

TABLE 8 Two-way ANOVA results for geometry and spar type.

Response variable	Factor	F-value	p-Value	Significance ($p < 0.05$)	Interpretation
Natural frequency	Geometry	6.63	0.124	⊗	Moderate influence
	Spar type	0.6	0.521	⊗	Minor influence
Deflection amplitude	Geometry	5.47	0.138	⊗	Strong mechanical trend
	Spar type	1.02	0.441	⊗	Weak influence

TABLE 9 NACA 4412 model, Characteristics and natural frequency, for 1st and 2nd modes.

Study	E, GPa	υ	ρ, kg/m^3	Cord length, m	Length, m	ω_{n1}, Hz	ω_{n2}, Hz
Mostakim et al. (2020)	69	0.33	2700	1	5	3.4568	21.448
Current work	69	0.33	2700	1	5	3.4637	21.53

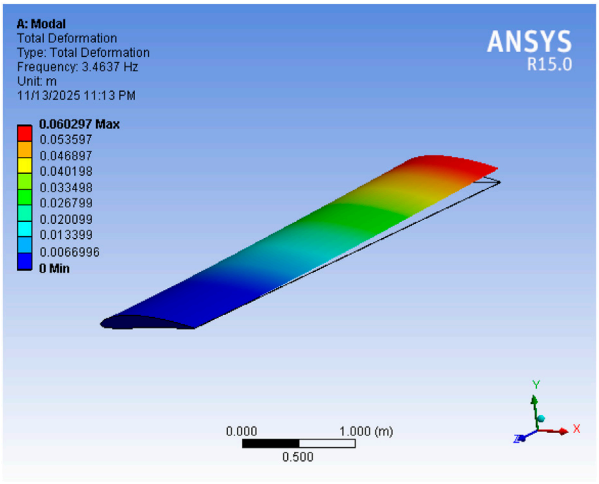

FIGURE 29
Simulation to the 1st mode vibration for reference (Mostakim et al., 2020).

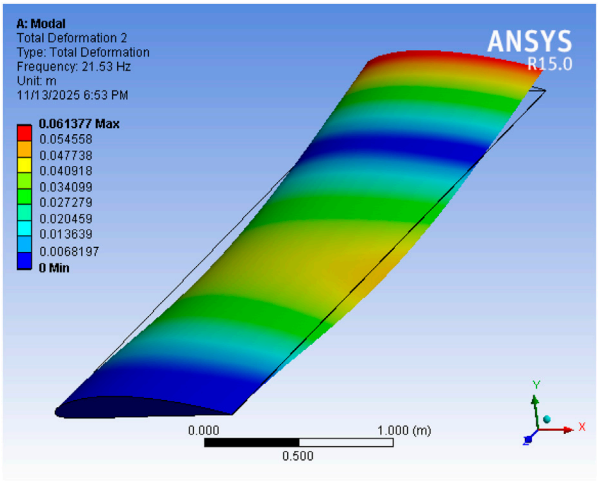

FIGURE 30
Simulation to the 2nd mode vibration for reference (Mostakim et al., 2020).

realistic aerodynamic excitations. Furthermore, experimental modal analysis and wind tunnel testing on scaled or composite prototypes are recommended to validate and calibrate the numerical findings. By combining these advanced numerical and experimental techniques, the present framework can be extended toward certification-level structural design, ensuring safer, more efficient, and dynamically robust aircraft wing systems.

10 Conclusion

The current research has studied how the wing geometry and structural configuration can affect the vibrational characteristics of aircraft wings, using the FEM. The six NACA profiles of airfoils were examined under two major planforms, tapered and swept-back, with box-spar and I-section spars. Modal and deflection analysis was conducted in order to find the natural frequencies and deformation. Further, two-way ANOVA was also done in order to verify the level of statistical significance of the differences in the results achieved. The principal conclusions obtained based on the findings are:

1. The tapered wings had greater natural frequencies than the swept-back wings in the six NACA investigated profiles. This is primarily because of the reduction in the effective spans and increased chordwise stiffness. The mean first mode frequency distribution of the tapered setup (9.75 Hz) was nearly 25% higher than the swept wings (7.3 Hz).
2. Box spar had 9.5%–22% and 20%–30% higher natural frequencies and deflection, respectively, compared to

I-section spars, and this demonstrates that Box configuration had better energy absorption and tortional resistance under dynamic loading in addition to showing greater flexibility. On the other hand, the I-section spars exhibited increased bending stiffness and reduced modal deflections especially at longer modal frequencies.

3. It was demonstrated that the effect of thicknesses of airfoils on dynamic stiffness was significant. Thickest profiles such as NACA 2424 were the most successful in capturing the highest natural frequencies of approximately 250 Hz in the sixth mode, and this indicates a positive relationship between rigidity and structural thickness.
4. Wings curvatures (camber) play a positive role on strengthen wings and increase their stiffness in terms of increasing natural frequency by 70%.
5. The finite element technique was also found to be very dependable and computationally efficient in estimating the vibration characteristics of airplane wings which gave a validated framework of initial aeroelastic and structural optimization.

Based on the obtained findings, it can be concluded that the tapered wings supported with I-section spars are the most favorable with weight efficiency, stiffness and vibration stability. In the other hand, swept box-spar configurations offer more flexibility beneficial for the high-speed applications. Since, the present work is limited to the linear elastic analysis; the nonlinear geometric and aeroelastic coupling effect might further affect the dynamic response. Also, further studies have to take into account the integrated Fluid-Structure Interaction (FSI) simulations as well as experimental modal testing in order to verify and extend these results under realistic flight conditions.

Data availability statement

The original contributions presented in the study are included in the article/supplementary material, further inquiries can be directed to the corresponding author.

Author contributions

NH: Conceptualization, Data curation, Formal Analysis, Validation, Visualization, Writing – original draft. AnA: Investigation, Resources, Writing – original draft. AS: Data curation, Investigation, Methodology, Writing – original draft. AAA: Data curation, Formal Analysis, Supervision, Validation, Visualization, Writing – original draft. AmA: Formal Analysis, Resources, Supervision, Writing – review and editing.

Funding

The author(s) declared that financial support was not received for this work and/or its publication.

Conflict of interest

The author(s) declared that this work was conducted in the absence of any commercial or financial relationships that could be construed as a potential conflict of interest.

Generative AI statement

The author(s) declared that generative AI was not used in the creation of this manuscript.

Any alternative text (alt text) provided alongside figures in this article has been generated by Frontiers with the support of artificial intelligence and reasonable efforts have been made to ensure accuracy, including review by the authors wherever possible. If you identify any issues, please contact us.

Publisher's note

References

Ahmed, S., and Ahmed, M. (2014). Modal analysis of thin walled multi-cell multi-tapered composite beams of closed cross sections. *Appl. Mech. Mater.* 629, 82–88. doi:10.4028/www.scientific.net/amm.629.82

Ahmed, F., Xiang, X., Wang, H., Zhang, J., Xiang, G., and Yang, S. (2025). Investigating wing-body lift interference effects on the dynamics of a novel flight-style AUV with bow-wings: maneuvering simulations and experimental validations. *Ocean. Eng.* 326, 120778. doi:10.1016/j.oceaneng.2025.120778

Andreson, J. D. (2011). *Fundamentals of aerodynamics, McGraw-Hill series in aeronautical and aerospace engineering*. McGraw-Hill.

Arunkumar, K. D., Lohith, N., and Ganesha, B. (2012). Effect of ribs and stringer spacings on the weight of aircraft structure for aluminum material. *J. Appl. Sci.* 12, 1006–1012. doi:10.3923/jas.2012.1006.1012

Banerjee, J. (2016). Modal analysis of sailplane and transport aircraft wings using the dynamic stiffness method. *J. Phys. Conf. Ser.* 721, 012005. doi:10.1088/1742-6596/721/1/012005

Basak, H., and Akdemir, A. (2024). Design optimization of cessna 172 wing with biomimetic design approach. *Int. J. Pioneer. Technol. Eng.* 3, 07–15. doi:10.56158/jpte.2024.66.3.01

Bennamia, I., Badereddine, A., and Zebbiche, T. (2018). Measurement of vibrations of composite wings using high-order finite element beam. *J. Measurements Engineering* 6, 143–154. doi:10.21595/jme.2018.20046

Campos, L., and Marta, A. C. (2013). "Fundamental bending frequencies of tapered wings," in *54th AIAA/ASME/ASCE/AHS/ASC structures, structural dynamics, and materials conference*, 1633.

Chan, Y. N., Harmin, M. Y., and Othman, M. S. (2018). Parametric study of varying ribs orientation and sweep angle of un-tapered wing box model. *Int. J. Eng. Technol.* 7, 155–159.

Choi, S., Park, K., Kim, J., Lee, S., and Lee, D. (2013). "Aeroelastic characteristics of high-aspect-ratio wing according to wing shape," in *51st AIAA aerospace sciences meeting including the new Horizons forum and aerospace exposition*, 143.

Demirtaş, A., and Bayraktar, M. (2019). Free vibration analysis of an aircraft wing by considering as a cantilever beam. *Selçuk Üniversitesi Mühendislik, Bilim Ve Teknol. Derg.* 7, 12–21. doi:10.15317/scitech.2019.178

Doğan, N. F., and ŞahİN, B. (2021). Comparative study on the vibration behavior of aluminum alloys used in aerospace applications. *Structure* 12, 16.

Elshazly, E., Kassem, M., and Elshafei, M. (2025). Aeroelastic coupled mode behavior of swept composite wing. *J. Phys. Conf. Ser.* 3070, 012001. doi:10.1088/1742-6596/3070/1/012001

Farsadi, T., and Hasbestan, J. (2019). Calculation of flutter and dynamic behavior of advanced composite swept wings with tapered cross section in unsteady incompressible flow. *Mech. Advanced Materials Structures* 26, 314–332. doi:10.1080/15376494.2017.1387322

Guo, S., Cheng, W., and Cui, D. (2006). Aeroelastic tailoring of composite wing structures by laminate layup optimization. *AIAA Journal* 44, 3146–3150. doi:10.2514/1.20166

He, Y., Wang, J., Li, J., Duan, B., Zhou, Y., and Wang, K. (2023). Effect of aeroelastic tailoring design on wing mode. *Int. J. Aerosp. Eng.* 2023, 1711088. doi:10.1155/2023/1711088

Hongwei, W., and Mao, Y. (2008). Dynamic analysis on high aspect ratio composite wing. *Comput. Aided Eng.* 17, 21–23.

Hoy, M., Samrandee, V., Samrandee, W., Suddeepong, A., Phummiphan, I., Horpibulsuk, S., et al. (2023). Evaluation of asphalt pavement maintenance using recycled asphalt pavement with asphalt binders. *Constr. Build. Mater.* 406, 133425. doi:10.1016/j.conbuildmat.2023.133425

Jaafar, A. S., and Hmoad, N. R. (2024). The effect of formal specifications and working conditions on the resistance and vibration of the NACA 4415 aircraft wing model. *Eng. Technol. and Appl. Sci. Res.* 14, 18147–18152. doi:10.48084/etasr.8547

Jha, R., Chattopadhyay, A., Jha, R., and Chattopadhyay, A. (1997). "Development of a comprehensive aeroelastic analysis procedure for composite wings using laplace domain methodology," in *38th structures, structural dynamics, and materials conference*, 1026.

Jonsson, E., Riso, C., Monteiro, B. B., Gray, A. C., Martins, J. R., and Cesnik, C. E. (2023). High-fidelity gradient-based wing structural optimization including geometrically nonlinear flutter constraint. *AIAA J.* 61, 3045–3061. doi:10.2514/1.j061575

Klimmek, T., and Schwochow, J. (2001). *Geometric and structural sensitivity analysis of aeroelastic characteristics of wings.*

Krishna, K. R., Jadhav, S. D., and Mishra, A. K. (2023). *Comparative modal analysis on different aircraft wing models.*

Liu, T. (2021). Evolutionary understanding of airfoil lift. *Adv. Aerodynamics* 3, 37. doi:10.1186/s42774-021-00089-4

Miskin, D. L., and Takahashi, T. T. (2019). Preliminary design of a wing considering transonic aerodynamic, weight and aeroelastic behavior. *AIAA Aviat. 2019 Forum*, 3068.

Mostakim, Z., Mehfuz, N., Zabal, M. E., Sajib, K. A., and Hossain, M. Z. (2020). "Comparison of vibration analysis among NACA airfoil wings based on natural frequencies," in *International conference on mechanical, industrial and energy engineering*, 19–21.

Mousa, N. A., Attia, O. H., Mahmood, H. A., and Adam, N. M. (2022). Optimization efficiency of the aircraft wing of cessna 172 skyhawk by absorbent adverse pressure using tangential suction slot without vacuum device. *Math. Model. Eng. Problems* 9, 731–738. doi:10.18280/mmep.090320

Pagani, A., Petrolo, M., and Carrera, E. (2014). Flutter analysis by refined 1D dynamic stiffness elements and doublet lattice method. *Adv. Aircraft Spacecraft Science* 1, 291–310. doi:10.12989/aas.2014.1.3.291

Pany, C. (2023). Panel flutter numerical study of thin isotropic flat plates and curved plates with various edge boundary conditions. *Politeknik Derg.* 26, 1467–1473. doi:10.2339/politeknik.1139958

Pany, C., Parthan, S., and Mukhopadhyay, M. (2001). Free vibration analysis of an orthogonally supported multi-span curved panel. *J. Sound Vibration* 241, 315–318. doi:10.1006/jsvi.2000.3240

Patil, M., and Patil, M. (1997). "Aeroelastic tailoring of composite box beams," in *35th aerospace sciences meeting and exhibit*, 15.

Patuelli, C., Polla, A., Cestino, E., and Frulla, G. (2023). Experimental and numerical dynamic behavior of bending-torsion coupled box-beam. *J. Vib. Eng. and Technol.* 11, 3451–3463. doi:10.1007/s42417-022-00759-7

Patuelli, C., Cestino, E., and Frulla, G. (2024). *Aeroelastic analysis through non-linear beam finite elements with bending-torsion coupling formulation.* Orlando, FL: AIAA SCITECH 2024 Forum, 1073.

Rajamurugu, N., Satyam, M., Nagendra, V., Yaknesh, S., and Sundararaj, M. (2024). Investigation of static aeroelastic analysis and flutter characterization of a slender straight wing. *Int. J. Automot. and Mech. Eng.* 21, 11203–11219. doi:10.15282/ijame.21.2.2024.3.0866

Sedaghati, R., Eng, P., and Elsayed, M. S. (2006). *Wing–box structural design optimization. Department of mechanical and industrial engineering conchordia university. Ref. No: CRIAQ.*

Srividhya, S., Nehru, K., Rago, A., and Selvan, P. (2020). Vibrational analysis of an aircraft wing model using ANSYS workbench. *Int. J. Eng. Dev. Res.* 8, 280.

Su, H., and Banerjee, R. (2018). The modal characteristics of high aspect ratio sailplane wings including the effects of bending and torsional rigidities. *J. Phys. Conf. Ser.* 1048, 012010. doi:10.1088/1742-6596/1048/1/012010

Viglietti, A., Zappino, E., and Carrera, E. (2017). "Free-vibration analysis of tapered wing structures using refined one-dimensional models," in *XVII international forum of aeroelasticity and structural dynamics* (Como, Italy: IFASD).

Nomenclature

a_0	Two-dimensional airfoil lift slope
AR	Aspect ratio
b	wing span m
C	Damping matrix. N.s/m
C_D	Coefficient of drag.
C_{D0}	Coefficient of drag at zero angle of attack
C_L	Coefficient of lift
C_r	Root chord lengths m
C_t	Tip chord lengths m
d	Displacement vector m
e	Oswald constant
E	Modulus of elasticity GPa
F	Variance
K	Stiffness matrix. N/m
MS	Mean square
p	Pressure. Pa
S	Surface area m^2
t	time s
u	Fluid velocity. m/s
um	Mesh velocity m/s
α	Angle of attack Degree
α_0	Zero lift angle of attack Degree
α_w	Sweep angle Degree
λ	Taper ratio
μ_f	Fluid viscosity $N.s/m^2$
ρ_f	Fluid density Kg/m^3
ρ_s	Structural density Kg/m^3
υ	Poisson's ratio Unitless
ω_n	Natural frequency Rad/s

Abbreviations

ANOVA	Analysis of variance
APDL	ANSYS Parametric Design Language
CFD	Computational fluid dynamics
CSV	Comma-separated values
FEM	Finite element method
f_{ext}	External aerodynamic loads.
FSI	Fluid- Structure Interaction
FFT	Fast Fourier transform
GVT	Ground vibration testing
NACA	National Advisory Committee for Aeronautics
UAVs	Unmanned aerial vehicles